The effect of fume on radiative heat transfer in kraft recovery boilers

RICHARD A. WESSEL, MARTIN K. DENISON, AND ARTIT SAMRETVANICH

ABSTRACT

A three-dimensional numerical model was used to evaluate the effect of fume on heat transfer in a kraft recovery boiler. The absorption and scattering efficiencies of fume particles were calculated from measurements of the complex refractive index of ash. Radiative properties of black liquor, char, and smelt particles were calculated based on correlations for emissivity as a function of temperature. Radiative properties of molten smelt and fume deposits on the furnace walls were approximated by emissivity correlations as a function of deposit surface temperature, incident radiation, and ash melting characteristics. Furnace heat transfer was modeled for a set of test conditions on a single-drum recovery boiler. Results presented include gas flow patterns, gas temperatures, dust concentrations, and radiative properties.

Application:

Numerical modeling of the optical and radiative properties of ash improves our ability to predict flow, combustion, and heat transfer.

Most of the heat transferred in a kraft recovery furnace is transferred by thermal radiation. Consequently, the radiative properties of combustion gases, particles (char, soot, and ash), and deposits on heat-transfer surfaces have a substantial effect on heat transfer rates. In turn, the heat transfer rates affect the boiler size and its efficiency. Considerable attention has been paid to the thermal properties of ash in coal-fired boilers (*1*, *2*), but the properties of ash in the combustion of kraft black liquor have been largely overlooked. The ash in a recovery boiler is mostly comprised of fume, which are aerosol particles formed by condensation of inorganic vapors in combustion gases.

Measurements were made recently of the radiative properties of recovery boiler ash (*3*, *4*). A three-dimensional mathematical model can be used to examine the effect of fume particles and deposits on heat transfer.

BACKGROUND

Traditionally, to specify boiler size and capacity, designers have relied on empirical methods based on decades of experience and field measurements. In **Table I**, coal-fired boilers and black liquor recovery boilers are compared in terms of typical design targets for gross heat input per plan area and for exit temperatures of furnace gases (*5*).

*The low melting point of the ash makes it necessary for the boiler to be large to absorb more heat, so the gas is at a lower temperature before it enters the convective section. Molten or sticky ash in the convective section can plug up the recovery boiler.

In black liquor recovery, the large quantity of ash and its low melting point* degrade the boiler's thermal efficiency. As a result, recovery boilers are much larger than coal-fired boilers, and recovery boilers require a larger capital investment per unit of heat input. Changes in firing practices, higher solids content in spent pulping liquors, and the effect of mill closure on potassium and chlorine levels in the ash have produced changes in heat transfer that are difficult to predict on the basis of previous experience.

The basic tools needed to calculate heat transfer in recovery boilers are (a) accurate measurements for radiation and heat conduction properties and (b) mathematical expressions to predict these thermal transport properties. Calculations of heat transfer can be used to optimize boiler design and operating conditions and to improve the thermal efficiency and capital effectiveness of the boiler.

Fundamental research is needed on characterizing the thermal transport properties of ash. Research of this kind is being supported by the American Forest and Paper Association and by the U.S. Department of Energy in its Agenda 2020 program (*6*).

RADIATIVE PROPERTIES

Values for the radiative properties of black liquor char, smelt, and ash are needed to calculate heat transfer in a recovery boiler. The diameters of particles of black liquor, char, and smelt from combustion of black liquor spray are commonly greater than 100 µm, which is larger than the wavelength of infrared radiation in the furnace. Therefore, properties of these particles can be approximated by the large particle limit for spherical particles, assuming that the emissivities of these materials are known.

Fume particles suspended in the flue gas are commonly oil to 10 µm and require measurements of complex refractive index to calculate radiative properties.

Gas-entrained particles

Values are needed for the properties of gas-entrained carryover and of aerosol particles (fume) to determine the absorption and scattering of radiation in the upper part of the furnace. Values for the complex

Type of fuel	Gross heat input/plan area		Exit gas temp.	
	MW_t/m^2	Btu/(h ft^2)	°C	°F
Coal-fired boilers				
Bituminous coal[a]	5.7	1.8×10^6	1300	2370
Lignite coal[b]	4.7	1.5×10^6	1050	1920
Black liquor	2.7	0.85×10^6	925	1700

[a]Low to medium slagging. [b]Severe slagging.

I. Design parameters for coal-fired boilers and black liquor recovery boilers (5)

index of refraction were recently measured to characterize the optical properties of pure Na_2CO_3, Na_2SO_4, K_2CO_3, K_2SO_4, and several samples of recovery boiler ash (*3*).

The complex refractive index was found to be dependent upon the amount of sulfate and carbonate but independent of sodium and potassium. However, the values measured for the optical properties of recovery boiler ash did not vary significantly for samples of different composition. These measurements have made it possible to calculate total scattering and absorption efficiencies of fine particles of recovery boiler ash. The calculation of efficiencies is based on Mie theory, as applicable to homogeneous spherical particles (*7*) under the assumption that particles act as independent scattering sources.

The total efficiencies of recovery boiler ash particles as a function of temperature and particle diameter are shown in the graphs on the left side of **Fig. 1**. For comparison, the graphs on the right show the efficiencies for a low-iron coal ash calculated from optical constants measured by Goodwin (*8*). As the curves in the upper graphs show, the scattering efficiencies of the recovery boiler ash are similar to those of the coal ash. However, the absorption efficiencies of the recovery boiler ash are significantly lower than those of the coal ash, as the lower graphs show. For particle diameters on the order of 1 µm, the absorption efficiency of the recovery boiler ash is roughly ten times lower than that of coal ash.*

Even in relatively high concentrations (1–2% by wt.), inorganic material entrained by combustion gases in recovery furnaces does not significantly emit or absorb radiation compared to the radiation emissions and absorptions of H_2O and CO_2 gases. However, fume does affect radiative scattering, because fume has submicron aerosol particles that account for 0.5–2% of the gas weight.

Scattering reduces heat transfer to the furnace walls by contorting the path that a photon must travel to reach the wall. The amount of scattering depends on the concentration and the sizes of fume particles and is relatively independent of ash composition. Scattering increases as fume particles are generated by the condensation of inorganic vapors in the upper furnace and in the convective pass. Extensive scattering accounts for the low visibility in recovery boilers.

Furnace deposits

The spectral emittance values of kraft black liquor, dried solids, char, molten smelt, and fume deposits were recently measured, and total emittance was calculated as a function of blackbody temperature (*4*). Engineering correlations for total (spectrally integrated) emissivity and absorptivity were developed for these properties between temperatures of 100°C and 1800°C. The results are shown in **Fig. 2**.

As the curves show, black liquor, dried solids, and char have relatively high emissivities (0.8–1.0), and these values decrease with increasing temperature. Molten smelt also has a high emissivity (0.8–0.95). The emissivity of molten smelt is independent of the amount of sulfide oxidation, and molten smelt appears to be transparent to radiation at short wavelengths. Therefore, the emissivity of smelt must depend partly on the properties of the substrate. In other words, thermal radiation is transmitted through the smelt and is absorbed or reflected by the substrate.

Fume deposits have a low emissivity that decreases with the temperature of the radiation source, as the figure shows. Thin layers of submicron dust particles scatter and reflect radiation before it is transmitted to the substrate. The white color of fume deposits is characteristic of low emissivity (or high reflectivity) in the visible range of the radiative spectrum. Low emissivity reduces the transfer of heat to the surface wherever ash deposits are below the melting temperature and fume deposits are likely to collect. Similar behavior has been observed for coal ash (*2*) and other dielectric materials, in regard to total emissivity as a function of temperature.

Sintering is also believed to have significant effects on deposit thermal conductivity, emissivity, and surface heat transfer; however, these effects are just beginning to be measured (*6*).

RECOVERY BOILER MODEL

Flow and combustion

In this work, Babcock & Wilcox's Combustion Model for Process Recovery Boilers, COMO-PR[SM] has been used to simulate black liquor combustion in recovery boilers (*9–11*). The mathematical model is based on a fundamental description

COMO-PR[SM] is a service mark of Babcock & Wilcox.

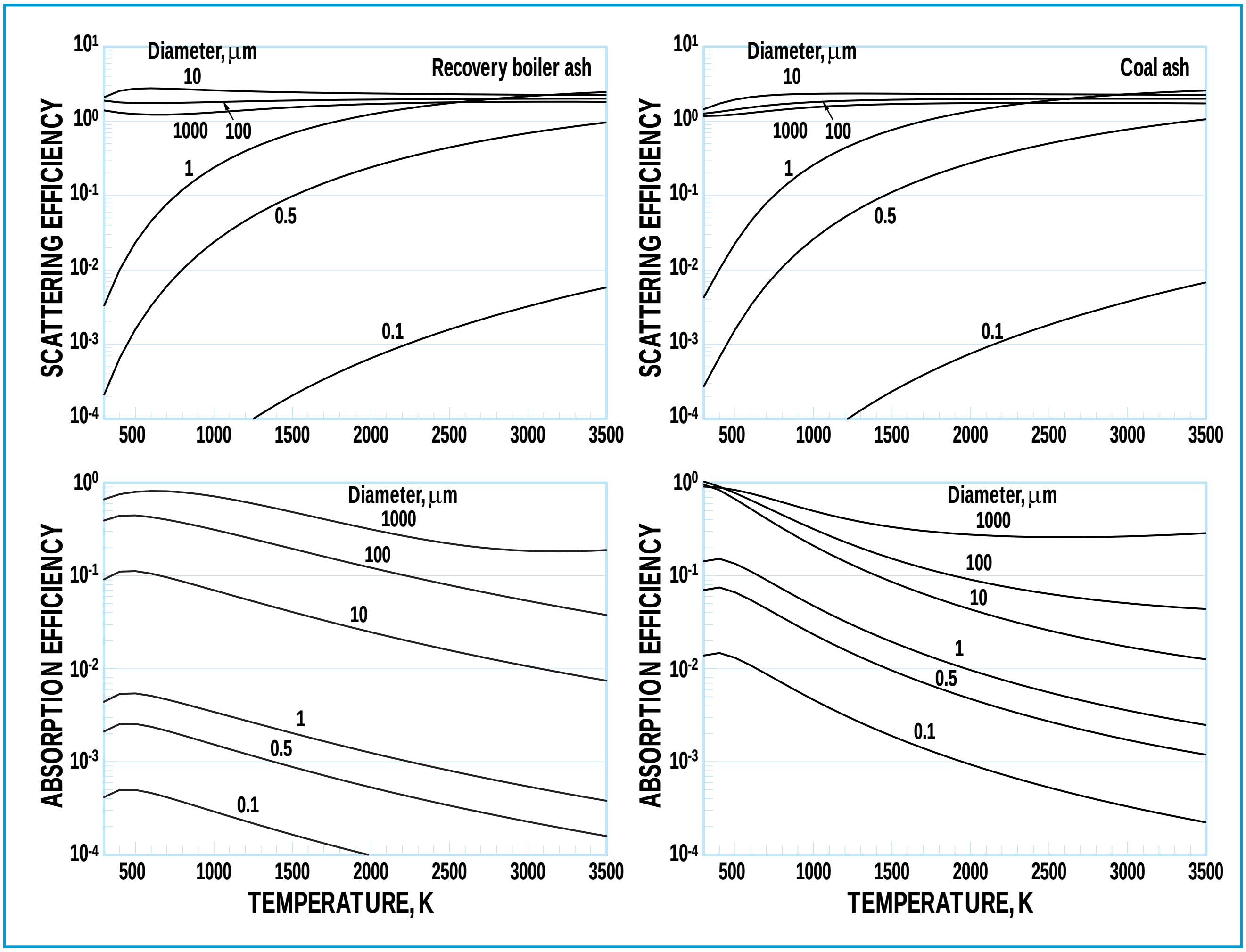

1. Calculated absorption and scattering efficiencies for spherical particles of recovery boiler ash [left, Sample D of Samretvanich (3)] and for spherical particles of coal ash [right, Sample SA01 from Goodwin (8)].

of various interacting processes of turbulent flow, chemical reaction, and heat transfer. Combustion is characterized in four stages: drying, devolatilization, char burning, and smelt oxidation.

The char-burning model includes mechanisms for alkali sulfate reduction, carbonate reduction, carbon removal by CO_2 and H_2O gasification, and combustion with O_2. The model for alkali release and fume formation includes mechanisms for physical ejection (micro explosions) of material from black liquor drops during drying and devolatilization, as well as mechanisms for sodium, potassium, and chlorine vaporization during char burning and smelt oxidation. The same reaction mechanisms are applied for black liquor spray, deposits on the furnace walls, and the active layer of the char bed. [For a critical review of recovery boiler modeling capabilities and needs, see the *TAPPI J.* article by Grace in 1996 (*12*)].

Radiative properties

The emission, absorption, and scattering properties of particle–gas mixtures are calculated based on the local temperature, the gas composition, the particle composition, and the particle number density. The absorption coefficient, *k*, includes contributions from both gas and

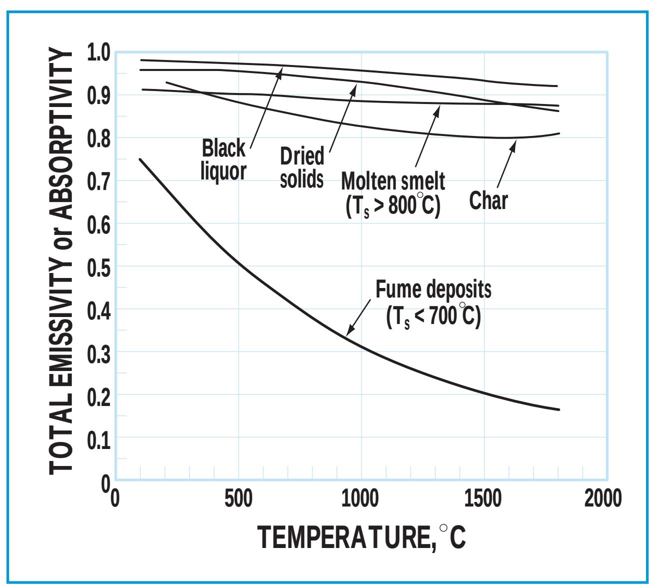

2. Emissivity correlations for black liquor, dried solids, char, molten smelt, and sintered fume deposits (4). The abscissa denotes the surface temperature, T_s, for total emissivity or the effective source temperature, T_b, for total absorptivity.

particles. The absorption coefficient of the gas mixture is calculated using Edwards's wide-band model (*13*).

The total absorption and scattering coefficients of the particles, k_p and σ_p, are calculated from absorption and scattering efficiencies:

$$k_p = \sum_i \frac{\pi}{4} d_i Q_{\text{abs},i} N_i \quad (1)$$

$$\sigma_p = \sum_i \frac{\pi}{4} d_i Q_{\text{sca},i} N_i \quad (2)$$

In each equation, the summation is over discrete particle size groups, where d_i is the particle diameter of size i, where $Q_{\text{abs},i}$ is the absorption efficiency and $Q_{\text{sca},i}$ is the scattering efficiency, and where N_i is the particle number density. Gas-entrained particles include burning black liquor drops, mechanical carryover, ejecta, and fume. The largest particles (>100 µm) of black liquor, char, and inorganic carryover are modeled by solving equations for the conservation of mass, momentum, energy, and chemical species in a Lagrangian reference frame. Efficiencies are calculated on the basis of the large-particle (optical) limit:

$$Q_{\text{abs}} = \varepsilon \quad (3)$$

$$Q_{\text{sca}} = 1 - \varepsilon \quad (4)$$

The emissivity, ε, is calculated from correlations in Fig. 2 (*4*). The particle diameter is calculated from correlations of drop size distribution from a splash plate nozzle (*14*). A particle is assumed to swell to roughly three times its initial diameter at the end of devolatilization and then to shrink at a rate that depends on the extent of carbon removal during char burning.

Particles of intermediate size (1–100 µm) are formed by physical ejection from burning black liquor drops. Ejecta particles are modeled by equations being solved for the conservation of mass and chemical components in an Eulerian reference frame. The diameters of ejecta are assumed to be uniform, each particle with an initial size of 30 µm, and the swelling characteristics are assumed to be the same as those of large particles. The efficiencies are calculated from the large-particle limit for the short span during which char burning occurs. After char burning, the efficiencies in Fig. 1 are used for spherical particles of recovery boiler ash.

Fume particles are typically 0.1–1 µm in diameter. These particles are also modeled by equations being solved for the conservation of mass and chemical components in a Eulerian reference frame. The local quantity and composition of fume are determined from multiphase chemical equilibrium between gas-phase combustion products and volatile sodium, potassium, and chlorine. Fume particles are assumed to be of uniform diameter (1.0 µm), and the ash particle efficiencies shown in Fig. 1 are used.

All heat transfer surfaces in a recovery boiler are covered with inorganic deposits (frozen smelt, molten smelt, and fume) of various thicknesses and densities. The emissivities and absorptivities of furnace wall deposits are calculated based on the local surface temperatures and melting properties of ash using the correlation shown in Fig. 2. The surface temperature is used in the correlation for calculating total emissivity, and an effective source temperature for incident radiation is used in the correlation for calculating total absorptivity. The effective source temperature was calculated from the incident radiative flux, q_{inc}, as follows:

$$T_b = \left(\frac{q_{\text{inc}}}{\sigma} \right)^{1/4} \quad (5)$$

where σ is the Stephan–Boltzman constant.

The correlation for char is used wherever black liquor is depositing and burning on the walls; otherwise, the correlation for smelt or fume deposits is used. When deposit surface temperatures are less than 700°C, the properties of fume deposits are applied. Above 800°C, deposits are completely molten at the surface, and the properties of molten smelt are used. Between 700° and 800°C, deposits are highly sintered and are partially molten near the surface; therefore, properties are approximated by linear interpolation between the properties of fume and molten smelt.

Radiative heat transfer

Governing equations for radiative heat transfer are solved numerically, coupled with other equations for turbulent flow and combustion. The discrete ordinates method (*15*) is applied for an emitting–absorbing and scattering gray medium. The method accounts for nongray surfaces by evaluating total properties with an appropriate blackbody source temperature.

Radiative heat transfer to heat exchanger tubes was modeled by an additional contribution to the absorption and scattering coefficients in the tube regions. Tube banks are treated as a continuum, because it is impractical to resolve the individual tubes within the computational grid of the model. The effective radiative properties are calculated from tube diameter, spacing, and deposit emissivity.

Furnace heat transfer

Furnace heat transfer is determined with an equation for conservation of fluid enthalpy, where the fluid is a mixture of gases and fine particles (fume and ejecta). The flow rate and temperature of air entering the furnace define the inlet conditions. Sources of combustion products (water, volatiles, and char products) are added, from burning particles and char deposits on the furnace walls and char bed.

Heat absorbed by radiation from gases and fine particles and by convection on furnace walls and tube banks is included as a source or a sink in the enthalpy equation. Convective heat transfer to heat exchanger tubes is calculated with correlations for cross flow over the tube banks. The gas temperature distribution is finally determined from thermodynamic relationships of enthalpy, expressed as a function of the temperature and chemical composition of the fluid gas–particle mixture.

An energy equation for burning black liquor particles is solved in a Lagrangian reference frame. Particles exchange heat with their surroundings by radiation, convection, and mass transfer. The continuous distribution of particle size and velocity from each liquor nozzle is represented by a discrete number of particle streams. Each stream is characterized by an initial position, drop size, mass, velocity, temperature, composition, and number flow rate. Several thousand particle trajectories are calculated to determine the distribution of liquor spray, deposition on the furnace walls and char bed, and mechanical carryover leaving the furnace.

Heat transfer to the furnace walls is modeled based on a quasi-steady-state energy balance, as shown in **Fig. 3**, with variables defined in **Table II**. The model takes into account:

- Radiative and convection heat transfer to the surface
- Mass transfer by particle deposition
- Smelt run-off and sloughing of deposits
- Chemical heat release
- Conduction heat transfer through the deposits and tube metal to the boiling water in the tubes.

The energy balance was solved implicitly to predict heat absorption and surface temperature distribution on the furnace walls.

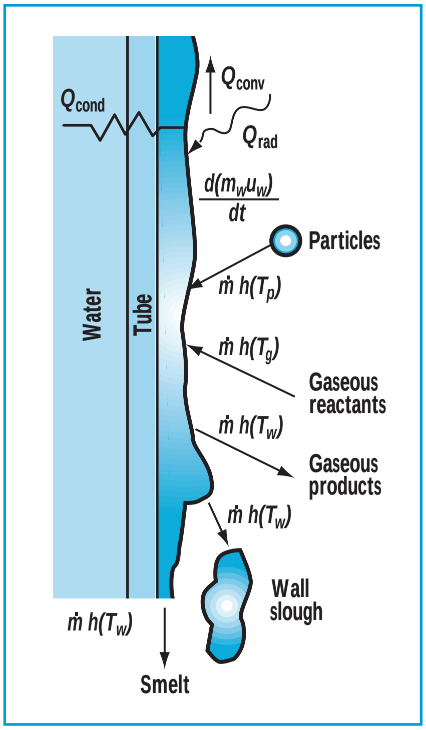

3. Energy balance on the furnace wall.

d/dt	=	derivative with respect to time, s^{-1}
$h(T_g)$	=	enthalpy evaluated at gas temperature, J/kg
$h(T_p)$	=	enthalpy evaluated at particle temperature, J/kg
$h(T_w)$	=	enthalpy evaluated at wall surface temperature, J/kg
m_w	=	mass of deposits on wall, kg/m^2
$\dot{m}$	=	mass flux, $kg/m^2 \cdot s$
Q_{cond}	=	conduction heat transfer rate, W/m^2
Q_{conv}	=	convection heat transfer rate, W/m^2
Q_{rad}	=	radiation heat transfer rate, W/m^2
u_w	=	internal energy of wall deposits, J/kg

II. Nomenclature for the variables in Fig. 3

Ash deposits on the furnace walls and superheater inlet are usually molten on the surface, a condition known as "slagging." Since values for the thermal properties and the distribution of deposits are not known, a minimum thermal conductance of 30–50 $W/(m^2 \cdot K)$ is assumed in the model. The surface energy balance is then solved for an estimated surface temperature and heat flux.

If the calculated surface temperature exceeds the melting temperature of the ash, then molten smelt flow counteracts deposit growth until deposit thickness and thermal conductance are in balance. In that case, the surface temperature is set equal to the ash melting point, and absorption heat flux and deposit thermal conductance are calculated from the surface energy balance.

The slagging boundary condition is a combination of two types of boundary conditions: constant thermal conductance and constant temperature. These two boundary conditions are commonly used for modeling furnace heat transfer, but they are always used independently. The advantage of the slagging boundary condition is that it is more realistic for simulating molten ash on furnace walls because it sets a practical upper limit on surface temperature and a lower limit on thermal conductance. If the ash composition and the actual melting temperature of the ash were known, then the melting temperature could also be permitted to vary based on local conditions on the wall.

RESULTS AND DISCUSSION

Boiler description

In this modeling study of furnace heat transfer, we used a recovery boiler that was experiencing problems with fouling and plugging of convection surfaces. The unit was a single-drum boiler with three levels of air injection and a sloping floor.

The boiler was tested during stable operation over an 8-h period. During testing, the boiler was firing liquor at a rate of 1476 metric tons of dry solids per day, which was approximately 87% of the manufacturer's rated capacity. The gross heat input per plan area at this load was 2.12 MW_t/m^2, which is below average for boilers of this size (mean = 2.5–2.7 MW_t/m^2). The boiler burns a mixture of black liquor from several mills. The amounts of chlorine and

Firing rate	
Dry solids flow rate, tons/day	1476
Gross heat input per plan area, MW_t/m^2	2.12
Liquor delivery	
Nozzles	4
Temperature, °C	123.3
Pressure, kPa	161.8
Air delivery	
Air flow rate, kg/h	258,120
Air flow distribution, %	
Primary	43.2
Secondary	30.1
Tertiary	26.7
Air temperature, °C	
Primary	162
Secondary	165
Tertiary	57
Boiler	
Drum	
Temperature, °C	280
Pressure, kPa(gauge)	6310
Main steam	
Temperature, °C	431
Pressure, kPa(gauge)	5771

III. Boiler operating conditions

potassium are usually higher than desired, which contributes to the plugging problems.

The conditions used during performance testing are summarized in **Table III**. Liquor was introduced to the furnace through two standard splash plate nozzles, one on the front wall and one on the rear wall, and through two wedge nozzles, one on each side wall. Liquor guns were oscillated vertically. At 123.3°C, the liquor was slightly above its boiling point and was flashing at the nozzle. Air flow was distributed at 43.2% to the primary air level, 30.1% to the secondary level, and 26.7% to tertiary air level.

Careful measurements of air flow distribution, damper settings, and liquor spray conditions were used to define the model. The model represents the geometry of the furnace enclosure, the superheater, and a portion of the long-flow generating bank. We represented air flow into the model by specifying the mass flow rate, the velocity, and the temperature at each inlet to the furnace. We represented liquor spray by specifying the particle-size distribution and the velocity leaving each nozzle.

Infrared video images of the char bed were recorded during boiler testing and were used to approximate the shape of the char bed in the model. The shape of the char bed was assumed to be fixed.

Geometrical parameters for the superheater and generating banks, including the number of tubes, tube spacing, and tube diameters, were accurately represented for predicting convection and radiative heat transfer and for estimating the draft loss.

Heat transfer results

The distributions of predicted flow and gas temperatures are shown in **Fig. 4** through the center planes in the furnace, front to rear and side to side. As the drawings on the left side of the figure show, the secondary air system creates opposing jets of air that collide in the center of the furnace. After colliding, these jets create a strong upward flow near the center and a downward flow near the side walls of the lower furnace. The flow becomes strongly biased to the left side of the upper furnace.

The two images on the right side of Fig. 4 show that there is a corresponding distribution of gas temperature in the upper furnace, with higher temperatures in regions of high upward flow. Side-to-side imbalances in gas flow and temperature cause an excessive amount of mechanical carryover that adversely affects the boiler performance. The model results were substantiated by observations of furnace brightness, carryover probing, and gas temperature measurements in the upper furnace.

Figure 5 presents a comparison of measured and predicted gas temperatures that occur at a horizontal plane above the bullnose. Measurements were made with a bare thermocouple wire inserted through inspection doors in the front wall, and the values were corrected for radiation losses. Predictions show more variation from front to rear and from left to right than the measurements reflected, but the average values are in good agreement. Disparities between measured and predicted temperature distributions may be caused by uncertainties in furnace operating conditions, in the flow distribution predicted, and in thermocouple measurements. Variations in deposit thickness and thermal properties on the furnace walls may also cause disparities between measured and predicted gas temperatures.

Figure 6 shows the concentrations of large and small particles in the furnace. The highest concentration of large particles, which include black liquor spray and carryover, is between the liquor guns and the char bed. The concentration of large particles decreases above the liquor guns. Of the particles that are carried upward, most fall back down as the char burns out and as smelt coalesces into smaller, denser particles.

The right side of the figure shows the distribution of concentrations of small particles, which include ejecta and fume particles. Ejecta particles are formed near the liquor guns as fine particles are ejected from burning black liquor drops. Fume particles start to form above the tertiary air level, and the concentration increases with decreasing gas temperature. Modeling results for fume formation and chemical composition are described elsewhere (*11*).

Figure 7 shows the distribution of total absorption coefficient and the distribution of scattering coefficient. The absorption coefficient includes contributions from gases and particles. The highest values are near the liquor guns where the concentrations of black liquor spray,

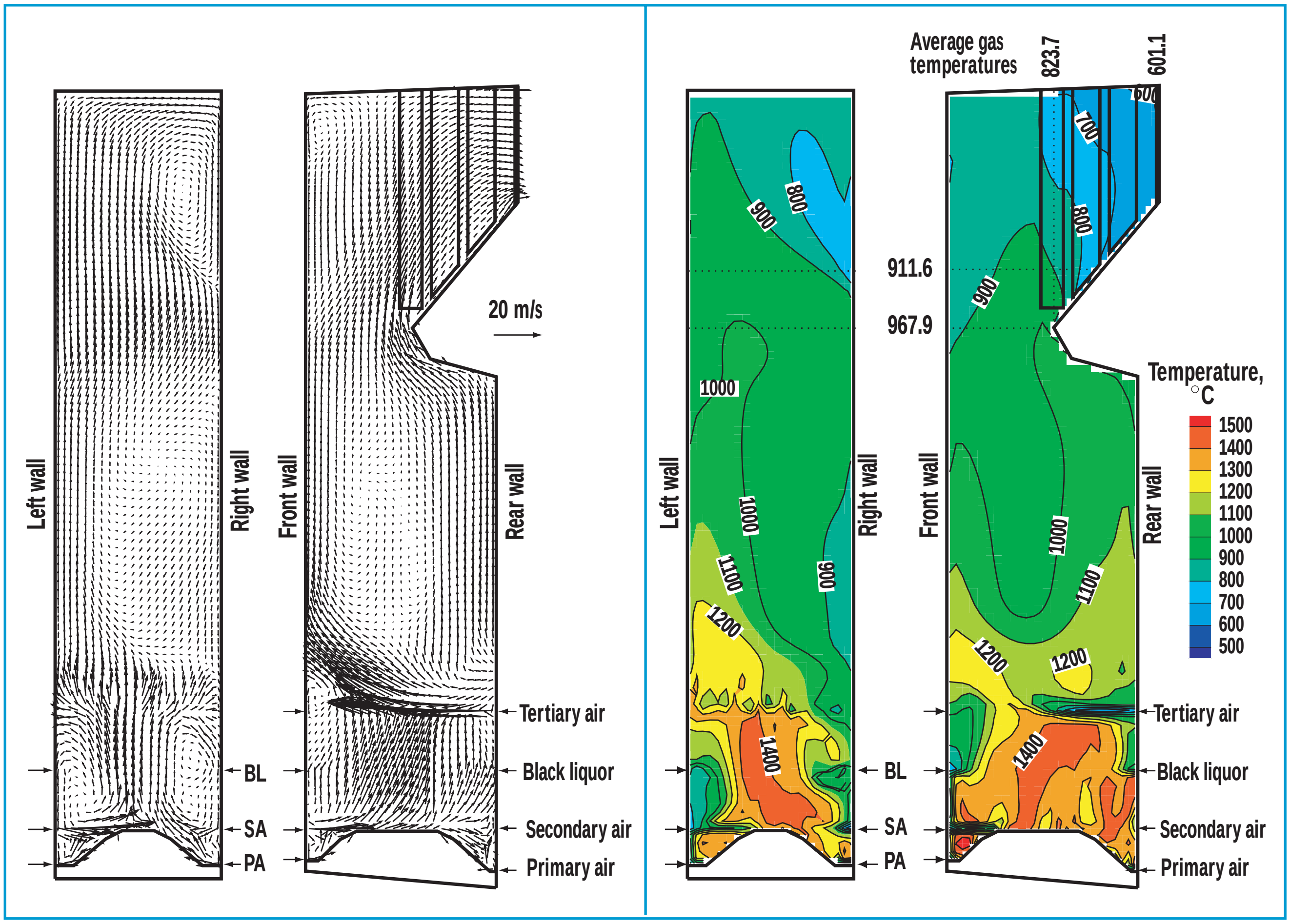

4. Flow patterns (left) and the distribution of gas temperatures (right) through the center planes of the furnace.

char particles, and ejecta are high. Gas-phase combustion products, H_2O and CO_2, dominate absorption throughout other parts of the furnace. As the right side of the figure shows, the distribution of scattering coefficients is dominated by the presence of fume. The coefficient values (~1 m^{-1}) are much higher than those for pulverized coal combustion (~0.1 m^{-1}). In the convection pass, the absorption and scattering coefficients include contributions from tube banks as a participating media.

The left side of **Fig. 8** shows the distribution of the rate of mass deposition, and the right side shows the distribution of the thermal conductance of deposits on the furnace walls. Black liquor spray, that is partly dried and combusted, deposits on the walls below the liquor guns, as the left side of the figure shows. Char deposits insulate the wall, resulting in a low thermal conductance, as shown on the right.

Molten smelt coats the walls of the middle and upper furnace. The

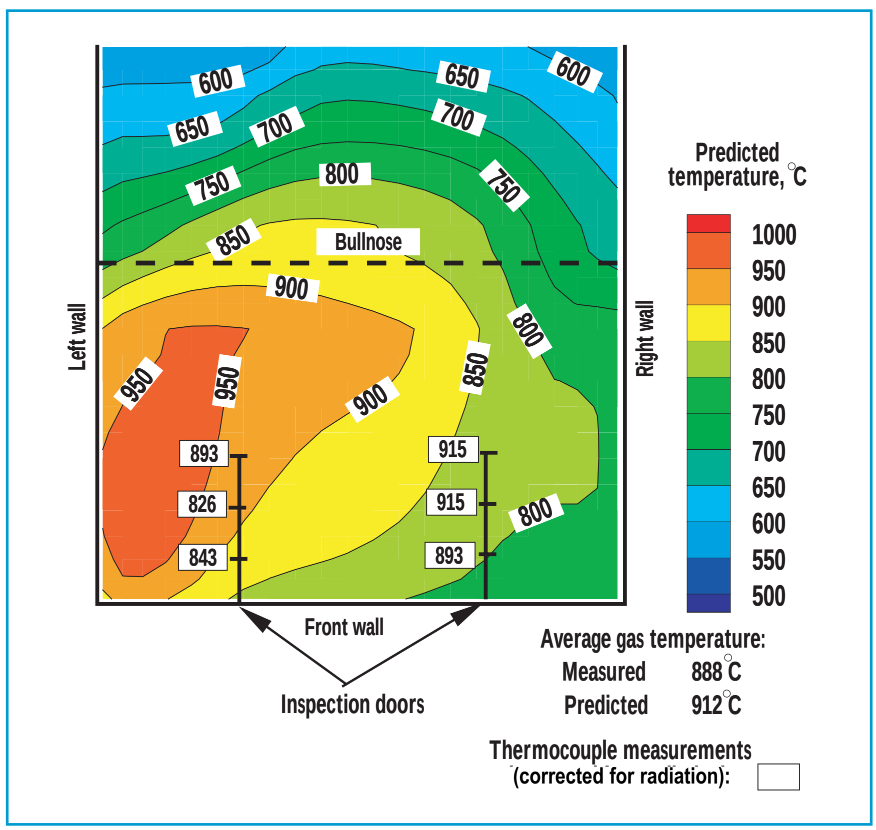

5. Measured and predicted gas temperatures at the horizontal plane above the bullose.

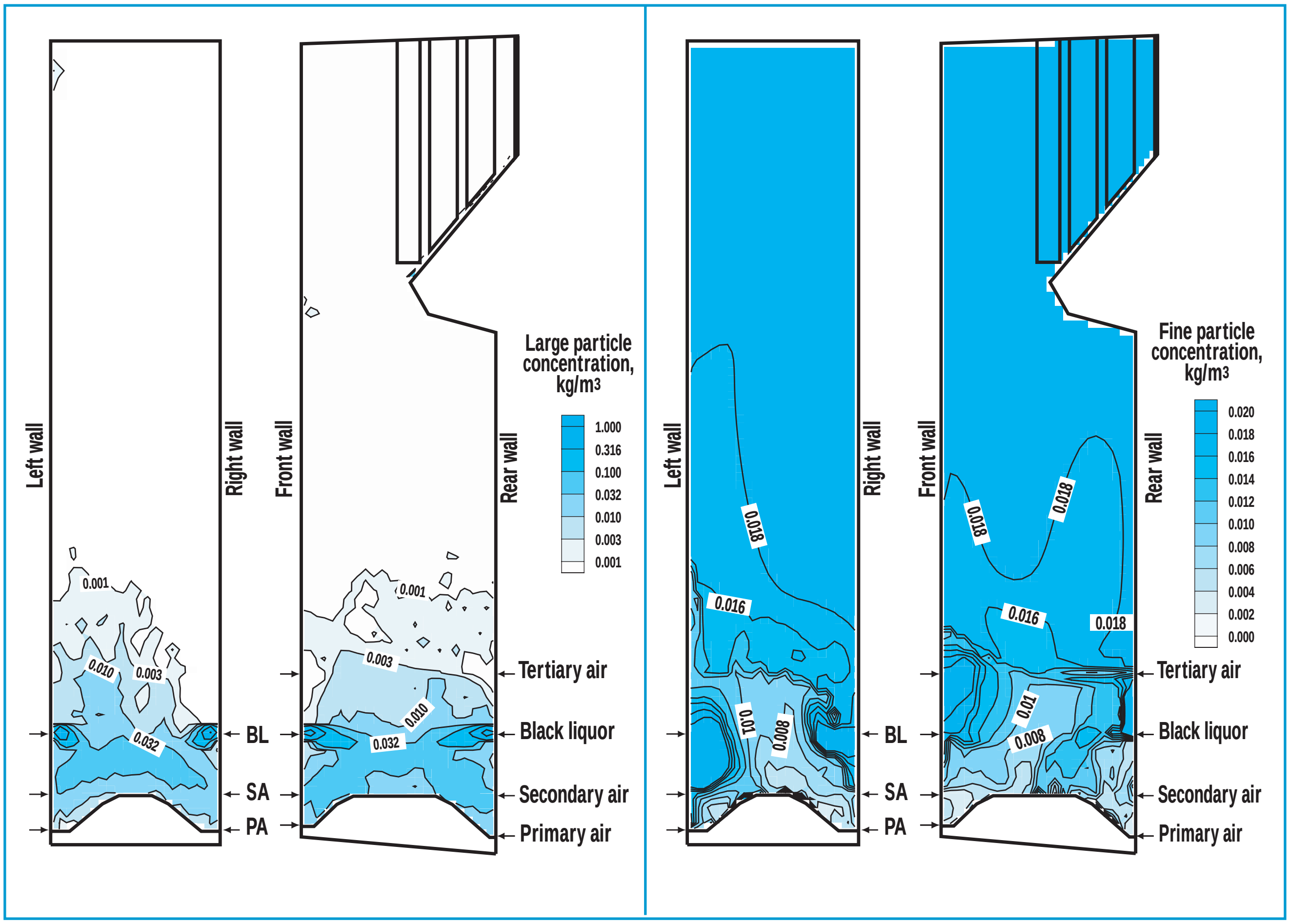

6. Distribution of the concentrations of large and fine particles through the center planes. Large particles include black liquor spray and carryover particles. Fine particles include ejecta and fume particles.

deposit conductance is dependent upon the local heat flux that is necessary to maintain the deposit surface at the melting temperature. On surfaces where the heat flux is high, deposits are thin, and the thermal conductance is high. Thermal conductance decreases with increasing elevation until the deposit surface temperature drops below the melting point, and dry fume deposits are likely to collect.

Figure 9 shows the distributions of deposit surface temperature and absorption heat flux on the furnace walls. The surface temperatures and heat flux are higher on the left side as a result of imbalances in gas flow and temperature. Molten smelt is present where surface temperatures are 800°C throughout most of the furnace. Fume deposits are present at lower surface temperatures that occur in the upper furnace and convection pass. Black liquor spray that impinges on the furnace walls near the black liquor guns reduces the surface temperature and the heat absorption because of the drying of black liquor and the build-up of char deposits in some areas. In other areas, char burning increases the surface temperatures.

Figure 10 shows the distributions of surface absorptivity and emissivity. In the lower furnace, where char and molten smelt are present on the furnace walls, values of absorptivity and emissivity are high (about 0.9). In the upper furnace and convection pass, where fume deposits are present, values are much lower (about 0.4). The figures show a sharp transition in the values at surface temperatures in the range of 700–800°C, which is the range through which melting occurs (Fig. 9, left). The transition from molten smelt to dry fume deposits also causes a decrease in absorption heat flux (Fig. 9, right), a physical transition that was observed and photographed during a boiler trip with oil firing.

Parametric effects

By scattering radiation, fume particles impede radiative heat transfer, causing a decrease in heat absorption and an increase in gas temperature at the furnace exit. If we neglect the effects of scattering by fume, the model shows an increase in furnace heat transfer and a decrease of approximately 55°C in average gas temperatures at the bullnose elevation. The effect of fume particle size is subtle. In the model, a change in fume particle diameter from 1 μm to 0.5 μm (and a corresponding increase in particle number density) causes the scattering coefficient to decrease from approximately 1.0 m^{-1} to 0.4 m^{-1} in the

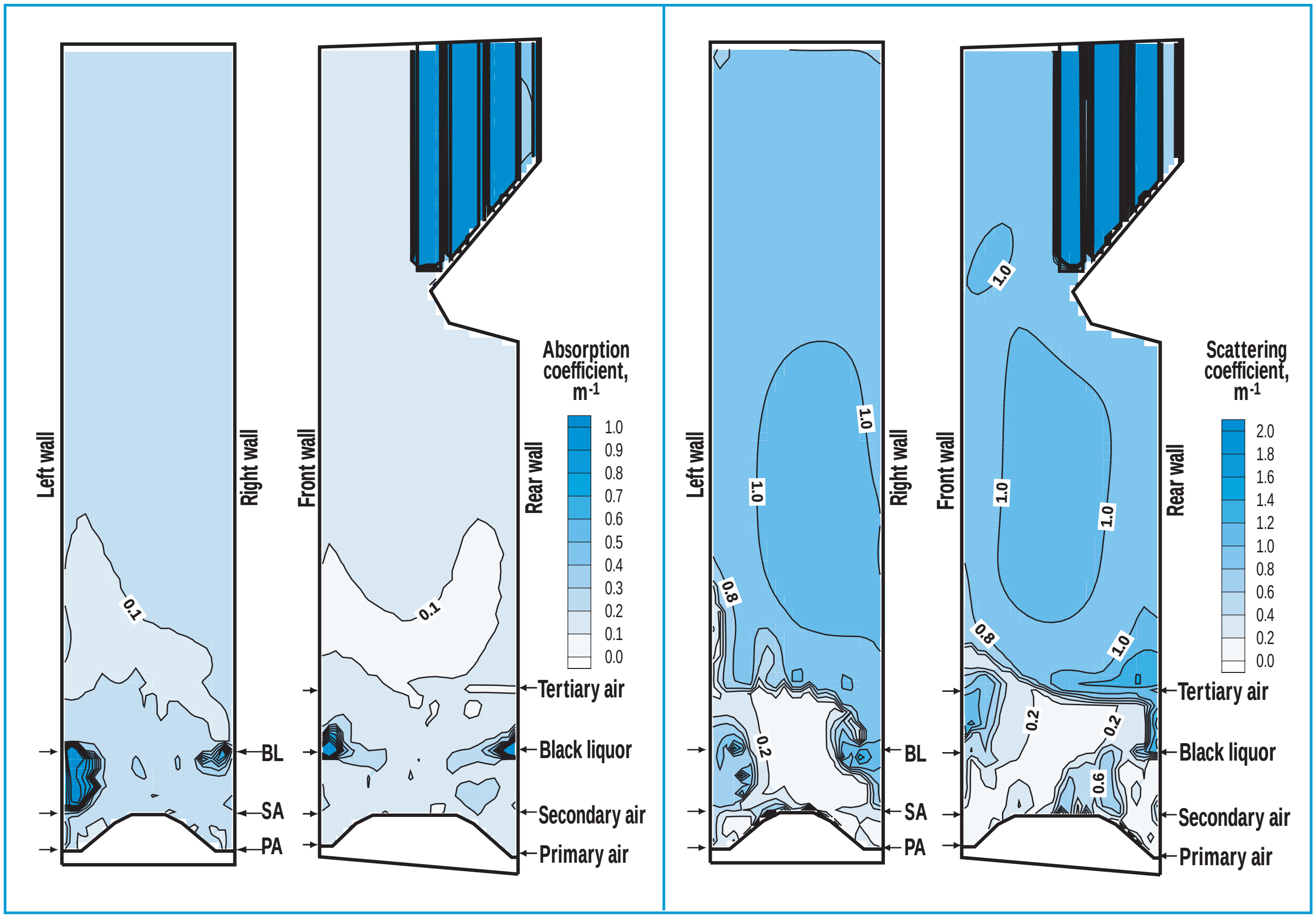

7. Distribution of absorption coefficients (left) and scattering coefficients (right) through the center planes.

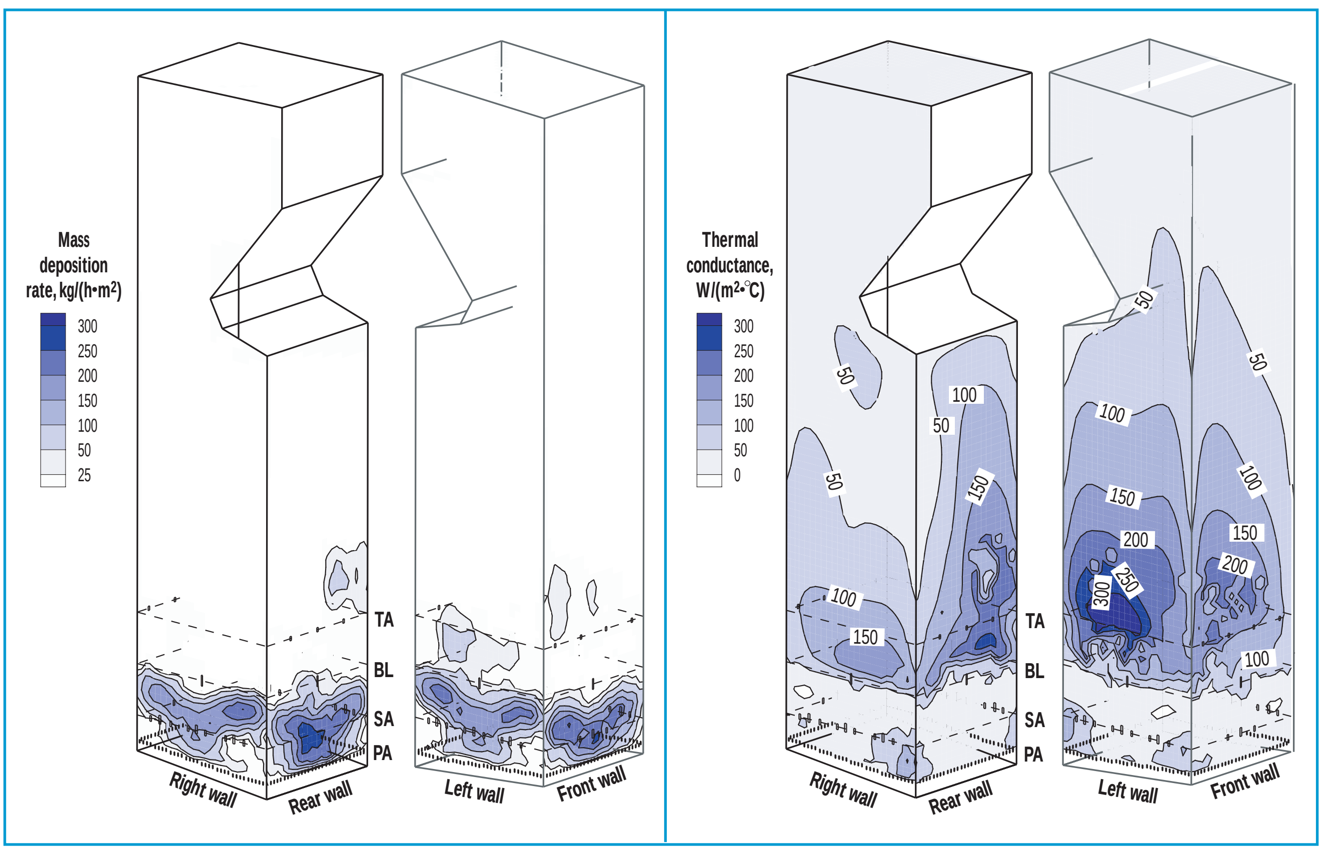

8. The rate of mass deposition (left) and the thermal conductance of deposits (right) on the furnace walls.

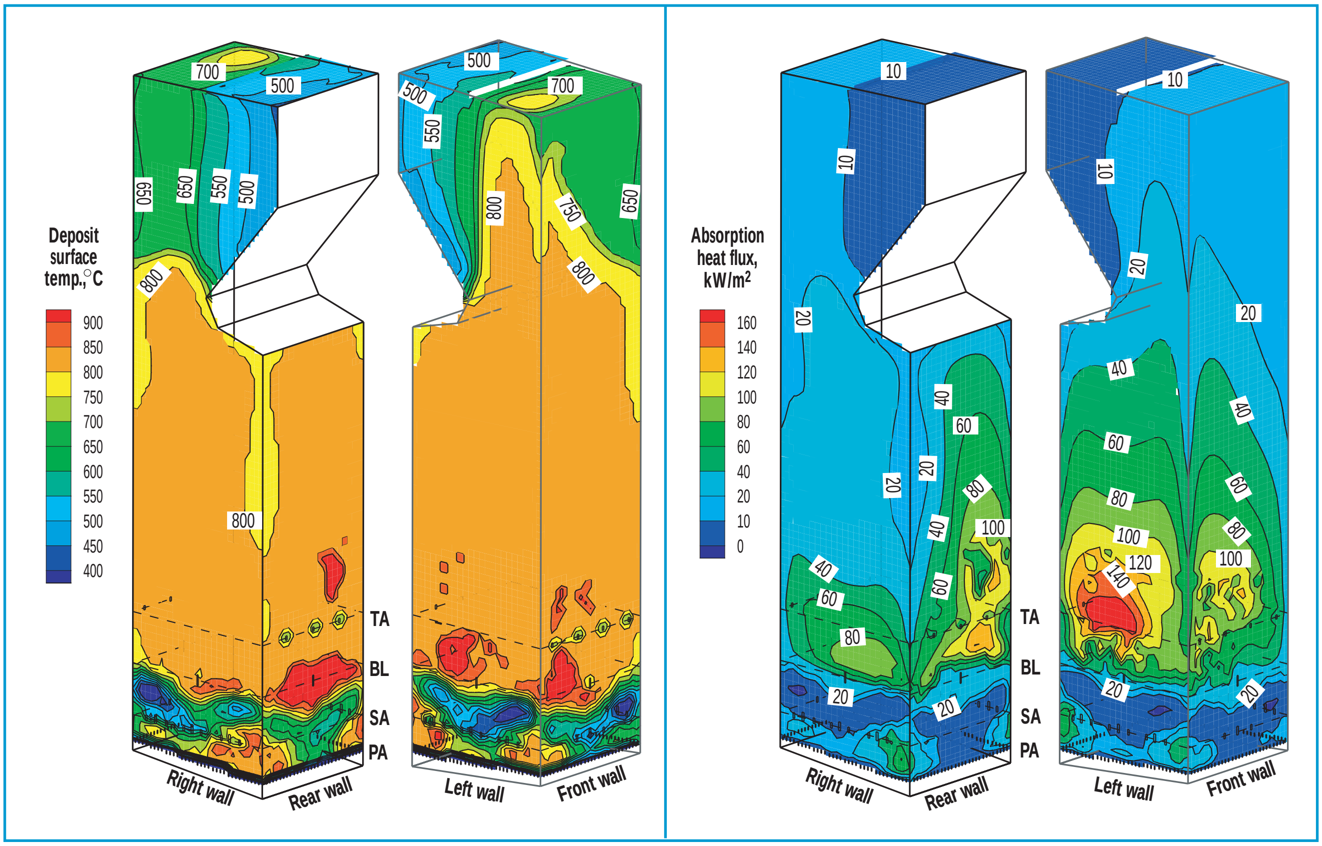

9. Deposit surface temperature (left) and absorption heat flux (right) on the furnace walls.

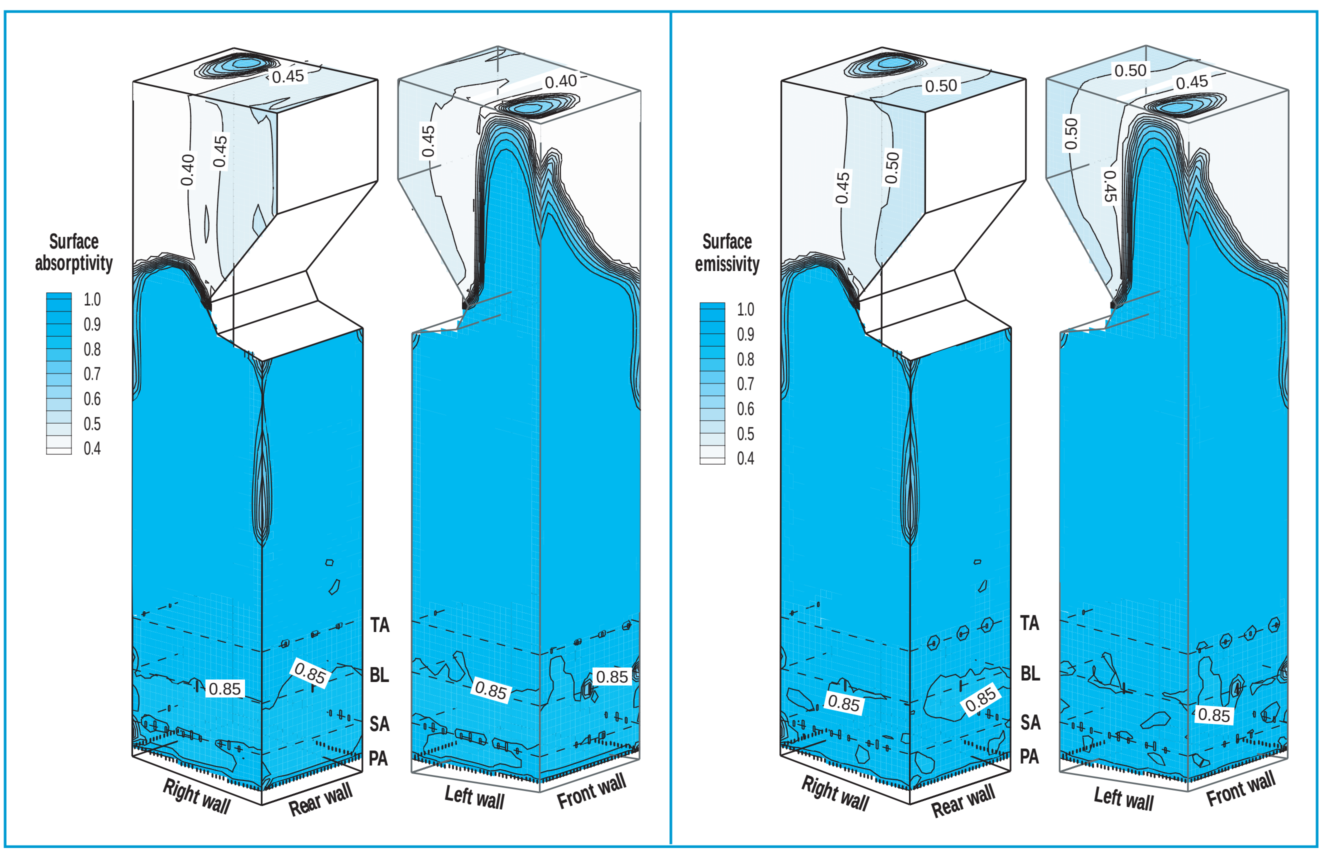

10. Surface absorptivity (left) and emissivity (right) on the furnace walls.)

upper furnace. The same change also causes the average, predicted gas temperature at the bullnose elevation to decrease by 12.4°C.

The thermal conductance of furnace wall deposits has the largest effect on furnace heat transfer, surface temperature, and absorption heat flux. A uniform thermal conductance was previously applied to the walls of the furnace and was adjusted in the model to match measurements of gas temperature at the furnace exit (*16*). The transition from molten smelt to dry fume deposits was predicted to occur at an elevation near the middle of the furnace. This prediction was not borne out by visual observations: molten smelt has been noted throughout most of the furnace. Therefore, thermal boundary conditions used in the current model are probably more realistic because the transition from molten smelt to dry fume deposits occurs much higher than reflected in the results obtained with previous models.

CONCLUSIONS

In a recovery boiler, heat transfer via radiation is impeded by radiation scattering from fume particles in the gas and by reflection from fume deposits on the upper furnace walls and the convection pass. The quantity of recovery boiler ash and its thermal properties substantially increase the furnace size over what it would be without ash. As a result, ash adds cost to the capital investment for a recovery boiler, which is much greater than the capital investment for a coal-fired boiler.

Measurements of the optical properties of recovery boiler ash and of the emissivity of fume deposits have improved our understanding of furnace heat transfer. As a result, we can more closely predict heat transfer performance. However, additional research is needed to determine the effects of carryover, deposition, fume deposition, and sintering on the thermal transport properties of deposits on the furnace walls and convection surfaces. TJ

Wessel is a principal engineer, and Denison was a research engineer at McDermott Technology, Inc., Research & Development Division, Alliance, Ohio. Samretvanich was a graduate student at Oregon State University, Dept. of Chemical Engineering, Corvallis, Oregon.

The authors thank the U.S. Dept. of Energy Office of Industrial Technology for financial support for measurements of the radiative properties of ash (DOE DE-FG02-90CE40936). We especially thank Tom Grace and Jim Frederick of the Institute of Paper Science and Technology. We also thank Larry Baxter of Sandia National Laboratories and Honghi Tran of the University of Toronto for their encouragement and technical support.

Received for review February 1998.
Accepted September 1998.
Presented at the TAPPI 1998 International Chemical Recovery Conference

LITERATURE CITED

1. Bryers, R. W., *Prog. Energy Combust. Sci*. 22: 29(1996).
2. Wall, T. F., Bhattacharya, S. P., Zhang, D. K., Gupta, R. P., and He, X., *Prog. Energy Combust. Sci*. 19: 487(1993).
3. Samretvanich, A., "Determination of the optical constants of ash samples from kraft recovery boilers," M.S. thesis, Dept. of Chemical Engineering, Oregon State University, 1997.
4. Wessel, R. A. and Bailey, R. T., "Radiative heat transfer properties for black liquor combustion," Babcock & Wilcox, DOE Topical Report, DE-FG02-90CE40936, August 1996.
5. *Steam, It's Generation and Use*, 40th edn. (S. C. Stultz and J. B. Kitto, Eds.), Babcock & Wilcox, Barberton, Ohio, 1992.
6. Baxter, L. L., Frederick, W. J., Wessel, R. A., and Tran, H., "Growth and property development of convection pass deposits in recovery boilers," annual report to the U.S. Dept. of Energy, Office of Industrial Technologies and the American Forest and Paper Association, Feb. 1998–Sept. 1998, Sandia National Laboratories, Oct. 2, 1998.
7. Bohren, C. F. and Huffman, D. R., *Absorption and Scattering of Light by Small Particles*, Wiley, New York, 1983.
8. Goodwin, D. G., "Infrared optical constants of coal slags," Ph.D. dissertation, Report No. T-255, High Temperature Gas Dynamics Laboratory, Dept. of Mechanical Engineering, Stanford University, July 1986.
9. Wessel, R. A., Parker, K. L., and Verrill, C. L., *Tappi Journal* 80(10): 207(1997).
10. Wessel, R. A. and Verrill, C. L., "Validation of combustion and fume formation models for an operating kraft recovery boiler," *TAPPI 1996 Engineering Conference Proceedings*, TAPPI PRESS, Atlanta, p. 775.
11. Wessel, R. A., Verrill, C. L., Blue, J. D., and Hiner, L. A., "Black liquor combustion model for predicting ash chemistry in kraft recovery boilers," proceedings of the AIChE 1998 Annual Meeting, AIChE, New York, Paper No. 291c.
12. Grace, T. M., *Tappi J.* 79(7): 182(1996).
13. Edwards, D. K., "Molecular Gas Band Radiation," in *Advances in Heat Transfer*, Vol. 12, Academic Press, New York, 1976, p. 115.
14. Empie, H. J., Lien, S. J., Yang, W. R., and Adams, T. N., *TAPPI 1992 International Chemical Recovery Conference Proceedings*, TAPPI PRESS, Atlanta, p. 429.
15. Fiveland, W. A., *J. of Thermophysics* 2(4): 309(1988).
16. Wessel, R. A., Denison, M. K., and Samretvanich, A., *TAPPI 1998 International Chemical Recovery Conference Proceedings*, Vol. 2, TAPPI PRESS, Atlanta, 1998, p. 425.